UNIVERSITY
OF TRENTO

DIPARTIMENTO DI INGEGNERIA E SCIENZA DELL'INFORMAZIONE

38123 Povo – Trento (Italy), Via Sommarive 14
http://www.disi.unitn.it

A CRACK IDENTIFICATION MICROWAVE PROCEDURE BASED
ON A GENETIC ALGORITHM FOR NON-DESTRUCTIVE TESTING

S. Caorsi, A. Massa, M. Pastorino

December 2001

Technical Report # DISI-11-010

A Crack Identification Microwave Procedure based on a Genetic Algorithm for Non-Destructive Testing

Salvatore Caorsi*, *Member*, *IEEE*, Andrea Massa**, and Matteo Pastorino**, *Senior Member*, *IEEE*

*Department of Electronics,

University of Pavia, Via Ferrata 1, 27100 Pavia - Italy

Tel. +39 0382 505661, Fax +39 0382 422583, E-mail: *caorsi@ele.unipv.it*

**Department of Biophysical and Electronic Engineering,

University of Genoa, Via Opera Pia 11/A, 16145 Genoa - Italy

Tel. +39 010 3532796, Fax +39 010 3532245, E-mail: *pastorino@dibe.unige.it,*
andrea@dibe.unige.it

Abstract - This paper is aimed at exploring the possibility of using a microwave approach based on a genetic algorithm to detect a defect inside a known host object. Starting from the knowledge of the scattered field, the problem solution is recast as a two step procedure. After defining a cost function depending on the geometric parameters of the crack, a minimization procedure based on a hybrid-coded genetic algorithm is applied. The influence of the noise as well as of the geometry of the defect on the crack detection and reconstruction is investigated. Moreover, the numerical effectiveness of the iterative approach is examined.

1   Introduction

The use of microwaves for material characterization and nondestructive testing and evaluation (NDT/NDE) is now rather common in several applications involving the inspection of dielectrics or conducting materials coated by dielectric layers. The reader can refer to papers [1][2][3][4] and references therein to have an idea of the directions followed by the research in this field. However, in the NDE community, microwaves are used in general to interrogate a sample and the information on the status of this sample is retrieved from transmission/reflection data. At the same time, deeper studies have been made concerning the potentialities of using microwaves as an imaging methodology in other areas (e.g., medical imaging [5]). Since the interaction of microwave and dielectrics with macroscopic dimension comparable with the wavelength gives rise to scattering phenomena, the information on the "image" of the object is contained in rather complex way into the scattered field. The resulting problem is higly nonlinear and ill-posed, and simple and efficient solution can be found only in particularly simple cases in which the object represents only a weak discontinuity in the propagating medium. In those cases, linearization techniques can be applied, which are usually based on Born-type approximations.

On the contrary, to inspect (for imaging purposes) stronger scatterers more complex iterative techniques (both deterministic and stochastic) must be used. It should be stressed that a number of iterative techniques have been proposed in recent years, essentially from researchers in the microwave community, who have no strong intersections with the NDE community. Those iterative procedures are usually very time consuming and, at present, are far from allowing a real or quasi-real time processing. Sometime, the use of parallel computers has also been suggested.

However, in the NDE area, a complete image of a scatterer may often constitute a redundant (although not undesired) information and a faster computation or a simplified processing is often preferred. In many cases the object to be inspected is completely

known except for a defect. The localization and shaping of the defect may constitute a sufficient information. Combining the above requirements with the efficiency of some of imaging-oriented methodologies, it is possible to develop a rather efficient tool for inspecting dielectrics in the NDE field.

In the authors' opinion, a key role for the choice of the methodologies most suitable to be "adapted" to the new problem in hand, is played by the possibility of including "a priori" information into the model. Concerning this point, stochastic approaches are usually superior to deterministic ones. Moreover, stochastic approaches are in principle able to get a global solution of the problem (the "correct" solution), whereas deterministic approaches can often be trapped in local solutions ("false" solutions). On the contrary, in imaging-oriented applications, deterministic approaches are usually much faster than stochastic methods. However, the time of convergence of these methods can be strongly reduced if the number of unknowns (which is of course very high in each imaging-based application) can be significantly limited, as it occurs in the presently proposed approach.

To this end, in the present paper we explore the possibility of using a stochastic procedure based on a genetic algorithm to detect defects in a known host object. A two-dimensional tomographic configuration is assumed and the defect is approximated by a void of fixed shape (rectangular). Position, dimensions and orientation of the defect inside the object cross-section are unknowns to be determined by measuring the scattered field. The inverse problem is reduced to an optimization one in which a suitable functional depending on only five geometric parameters defining the crack, have to be minimized. In this framework, genetic algorithms are very effective and reach the minimum (potentially, the global minimum) in a very short time.

In the following, the approach will be discussed and some results also for noisy environment provided, in which the main emphasis is on the correct defect localization and in the retrieval of its dimensions.

2 Mathematical Formulation

Let us consider a two dimensional geometry where a cylindrical inhomogeneous scatterer is embedded in a homogeneous external medium (Figure 1). The scatterer is characterized by a scalar permittivity $\varepsilon(x,y)$ and a conductivity $\sigma(x,y)$ and is successively illuminated by a number of known incident fields $\mathbf{E}_{inc}^v$, $v = 1, ..., V$. The working frequency is indicated by f_0. The incident fields are linearly polarized with the electric field directed along the axis of the scatterer: $\mathbf{E}_{inc}^v(\mathbf{r}) = E_{inc}^v(x,y)\mathbf{z}$ (TM polarization).

The scattered electric field, $E_{scatt}^v(x,y)$, (defined as $E_{scatt}^v(x,y) = E_{tot}^v(x,y) - E_{inc}^v(x,y)$, being $E_{tot}^v(x,y)$ the total field corresponding to the incident field $E_{inc}^v(x,y)$) is collected in an observation domain, S, external to the scatterer. The following integral equation holds:

$$E_{scatt}^v(x,y) = \int\int_D \tau(x',y')\, E_{tot}^v(x',y')\, G_{2D}(k_0\rho)\, dx'dy' \qquad (x,y) \in S \qquad (1)$$

where D is the object cross-section; $\tau(x,y)$ denotes the scattering potential defined as $\tau(x,y) = \varepsilon(x,y) - 1 - j\frac{\sigma(x,y)}{2\pi f_0 \varepsilon_0}$; G_{2D} is the two-dimensional free-space Green's function [6]; and $\rho = \sqrt{(x-x')^2 + (y-y')^2}$. The problem is that of detecting the presence of a void crack in the original scatterer. In more detail, we search for the position, the orientation and the size of a crack present in the original structure. The crack is approximated by an object of rectangular shape and parameterized by length, ℓ, width, w, orientation, θ, and center coordinates, (x_0, y_0) (Figure 1).

The approach used is a two step procedure, in which a detection phase precedes an identification phase. Firstly, we check whether there exists a crack in the structure by using the following object function:

$$\Phi_{detection} = \frac{1}{V}\sum_{v=1}^{V}\left\{\frac{\int\int_S \left|E_{scatt(cf)}^v(x,y) - E_{scatt(c)}^v(x,y)\right|^2 dxdy}{\int\int_S \left|E_{scatt(cf)}^v(x,y)\right|^2 dxdy} - \Omega_{noise}\right\} \qquad (2)$$

4

where $E^v_{scatt(cf)}(x, y)$ and $E^v_{scatt(c)}(x, y)$ are the scattered electric field measured in the observation domain for a crack-free case and when the defect is present, respectively; Ω_{noise} is a measure of the noise level defined as follows:

$$\Omega_{noise} = \frac{\int\int_S \left| E^v_{scatt(cf)}(x, y) - E^{v(noiseless)}_{scatt(cf)}(x, y) \right|^2 dxdy}{\int\int_S \left| E^{v(noiseless)}_{scatt(cf)}(x, y) \right|^2 dxdy} \tag{3}$$

where the super-script *noiseless* indicates the field values for the noise-free case. If the value of the object function is less than a fixed threshold η, then the investigated scatterer is assumed crack-free. Otherwise the identification phase starts. It should be pointed out that the value of the detection threshold is a function of the sensitivity of the measurement system.

The crack-identification problem is that of finding the parameters of the crack, x_0, y_0, w, θ. The object function when the defect is present is given by:

$$\tau_{(c)}(x, y) = \begin{cases} \tau_0 & if\ X \in \left[-\frac{\ell}{2}, \frac{\ell}{2}\right]\ and\ Y \in \left[-\frac{w}{2}, \frac{w}{2}\right] \\ \tau_{(cf)}(x, y) & otherwise \end{cases} \tag{4}$$

where $X = (x - x_0)\cos\theta + (y - y_0)\sin\theta$, $Y = (x_0 - x)\sin\theta + (y - y_0)\cos\theta$, $\tau_{(cf)}(x, y)$ and τ_0 are the object function for the crack-free geometry and for the void crack, respectively. Moreover, the electric internal field for the flaw configuration is unknown. We search for the array $\Psi = \{x_0,\ y_0,\ \ell,\ w,\ \theta;\ E^v_{tot(c)}(x, y)\}$ minimizing the following cost function:

$$\Phi_{identification}\{\Psi\} =$$

$$\frac{\alpha}{V} \sum_{v=1}^{V} \left\{ \frac{\int\int_S \left| E^v_{scatt(c)}(x, y) - \int\int_D \tau_{(c)}(x', y')\, E^v_{tot(c)}(x', y')\, G_{2D}(k_0\rho)\, dx'dy' \right|^2 dxdy}{\int\int_S \left| E^v_{scatt(cf)}(x, y) \right|^2 dxdy} \right\} +$$

5

$$\frac{\beta}{V} \sum_{v=1}^{V} \left\{ \frac{\int \int_D \left| E_{inc}^v (x,y) - E_{tot(c)}^v (x,y) + \int \int_D \tau_{(c)} (x',y') E_{tot(c)}^v (x',y') G_{2D} (k_0 \rho) dx'dy' \right|^2 dxdy}{\int \int_S \left| E_{inc}^v (x,y) \right|^2 dxdy} \right\}$$

<div align="right">(5)</div>

The first term is the normalized error in fitting the measured data (Φ_{data}); the second term is a measure of the error in satisfy the state equation (Φ_{state}); α and β are two regularizing constants.

By the Richmond method [7], the following discretized version of the functional (4) is obtained:

$$\Phi_{identification} \{\psi\} =$$

$$\frac{\alpha}{MV} \sum_{v=1}^{V} \sum_{m=1}^{M} \left\{ \frac{\left| E_{scatt(c)}^v (x_m,y_m) - \sum_{n=1}^{N} \tau_{(c)} (x_n,y_n) E_{tot(c)}^v (x_n,y_n) \int_{D_n} G_{2D} (k_0 \rho_{mn}) dx'dy' \right|^2}{\left| E_{scatt(c)}^v (x_m,y_m) \right|^2 dxdy} \right\} +$$

$$\frac{\beta}{NV} \sum_{v=1}^{V} \sum_{n=1}^{N} \left\{ \frac{\left| E_{inc}^v (x_n,y_n) - E_{tot(c)}^v (x_n,y_n) + \sum_{p=1}^{N} \tau_{(c)} (x_p,y_p) E_{tot(c)}^v (x_p,y_p) \int_{D_p} G_{2D} (k_0 \rho_{np}) dx'dy' \right|^2}{\left| E_{inc}^v (x_n,y_n) \right|^2 dxdy} \right\}$$

<div align="right">(6)</div>

where $\psi = \left\{ x_0, y_0, \ell, w, \theta; E_{tot(c)}^v (x_n,y_n), n = 1, ..., N \right\}$; (x_n, y_n) denotes the center of the n-th discretization domain; (x_m, y_m) indicates the m-th measurement point; ρ_{ij} is the distance between the i-th and j-th centers and D_l the area of the l-th sub-domain. The considered problem discretization suggests the assumption that ℓ, w, θ belong to finite sets of values: $\ell \in \{L_j, j = 1, ..., L\}$, $w \in \{w_i, i = 1, ..., W\}$, $\theta \in \{p\Delta\theta, p = 1, ..., P\}$. In particular, ℓ and w are multiple of the side of the discretization cell and θ of the angular step used for the multiview process.

$\Phi_{identification} \{\psi\}$ is minimized by an iterative procedure able to generate a sequence of trial configurations $\psi^{(k)}$, $k = 1, ..., K$, being k the iteration number, which converges to the extremum of the functional. Because of the nature of the unknowns, it is necessary

to choose a method able to treat simultaneously discrete and continuous variables. Moreover, due to the nonlinearity of the functional (the nonlinearity arises from the multiple scattering phenomena), an algorithm able to avoid local minima is necessary. A GA [8] seems to be a good choice. In general, GAs have demonstrated their effectiveness in treating nonlinear function with many unknowns [9] and avoiding the solution to be trapped in local minima.

3   Application of the Genetic Algorithm

Genetic algorithms [8][10][11][12] are efficient and robust population-based search and optimization techniques. An individual in a GA population (called *chromosome*) is a finite-length string code corresponding to a solution of a given problem (in our case, ψ). Each individual has a fitness value (in our case, $\Phi_{identification}\{\psi\}$) associated with it, that is a measure of its closeness to the actual solution. Iteratively, an initial population of N_P individuals (*population size*) evolves through successive generations by the application of genetic operators namely, selection, crossover and mutation until some termination criterion is satisfied.

In order to design a genetic algorithm for a specific problem the following points must be taken into account:

1. An encoding procedure must be defined in order to provide a one-to-one mapping between the parameter space and the chromosomes;

2. Variation operators must be defined that obey the mathematical properties of the chosen representation and permit to create new individuals starting from the existing ones;

3. A termination criterion is needed.

This section describes the choices considered when a genetic algorithm is applied for the identification of a crack.

3.1 *Encoding Procedure*

In general, GAs use a binary representation of the individuals as fixed-length strings over the alphabet $\{0, 1\}$ [10], such that they are well suited to handle pseudo-Boolean optimization problems. For optimization problems with discrete parameters, an integer-valued parameter is typically represented by a string of q bits, where $q = log_2\Theta$, being Θ the number of values that the discrete variable can assume. In this work, ℓ, θ, and w, are coded in binary strings of $Q = log_2L$ bits, $T = log_2P$, and $R = log_2W$, respectively. Moreover, after discretization of the investigation domain, also the center coordinates of the crack are considered as discrete parameters, then x_0 and y_0 are represented with $C = log_2N_l$ bits, where $N_l = \sqrt{N}$. For simplicity, a square cross-section is assumed.

Furthermore, a real-valued representation is used for the electric field $E_{tot(c)}^v\left(x_n, y_n\right), n = 1, ..., N$. This choice seems to be particularly suitable in this case [13][14][15][16]. The use of the floating-point representation for real unknowns results in a reduction of the computational load (the binary coding/decoding procedure is avoided) without violating the algorithmic framework [17]. Then each unknown array results in a hybrid-coded individual (*chromosome*) obtained concatenating the code of each parameter (*gene*), as shown in Figure 2.

3.2 *Genetic Operators*

Binary tournament selection [18] and binary double point crossover [19] are used for selection and crossover, respectively. Then, the mutation is performed with probability P_m on an individual of the population. This mutation consists in perturbing, according to

an assigned probability function P_{bm}, only one element of the chromosome. If the element is a bit, it is changed from zero to one or viceversa; otherwise the following mutation rule is considered

$$\Im\left\{E_{tot(c)}^{v(k+1)}\left(x_n, y_n\right)\right\} = \begin{cases} \Im\left\{E_{tot(c)}^{v(k)}\left(x_n, y_n\right)\right\} + \\ r\left|max_n\left[\Im\left\{E_{tot(c)}^{v}\left(x_n, y_n\right)\right\}\right] - \Im\left\{E_{tot(c)}^{v(k)}\left(x_n, y_n\right)\right\}\right| \\ \qquad if\ p \geq 0.5 \\ \\ \Im\left\{E_{tot(c)}^{v(k)}\left(x_n, y_n\right)\right\} - \\ r\left|\Im\left\{E_{tot(c)}^{v(k)}\left(x_n, y_n\right)\right\} - min_n\left[\Im\left\{E_{tot(c)}^{v}\left(x_n, y_n\right)\right\}\right]\right| \\ \qquad otherwise \end{cases} \quad (7)$$

where $\Im\left\{\right\}$ indicates the imaginary or the real part; r and p are random values belonging to the range $[0, 1]$, with a uniform distribution generated by a pseudo-random number generator; $(min_n\Im\left\{E_{tot(c)}^{v}\left(x_n, y_n\right)\right\}$; $max_n\Im\left\{E_{tot(c)}^{v}\left(x_n, y_n\right)\right\})$ is the acceptance domain for the unknown $\Im\left\{E_{tot(c)}^{v}\left(x_n, y_n\right)\right\}$.

3.3 *Termination Criterion*

Since the amount of computing time required to obtain solution of a desired quality is not known *a-priori*, the halting criterion for the iterative algorithm is taken to be a certain maximum number of generations (K_{max}), or when a fixed threshold (ξ) for the fitness function is achieved $(\Phi_{identification}\left\{\psi\right\} \leq \xi)$.

In this work, in order to keep the population diversity among new generations and avoiding a premature convergence, we define a new procedure called *refresh step*. This is carried out whenever the fitness difference between the fittest and weakest individuals of the population is below a specified trigger level, γ (i.e., a measure of the premature

convergence for the algorithm) or when the value of the optimal fitness is stationary for more than $K_0 = 0.1 K_{max}$ generations. Starting from the best individual generated, $\psi^{(opt)} = \{ x_0^{(opt)}, y_0^{(opt)}, \ell^{(opt)}, w^{(opt)}, \theta^{(opt)}, E_{tot(c)}^{v(opt)}(x_n, y_n), n = 1, ..., N \}$, we generate a new population according to the following rules:

- the best individual is copied into the new population;

- $\frac{N_p}{2}$ individuals are randomly generated inside the search space

- one chromosome (called *Born-type* chromosome) is generated. The first B-bits are the same of the best individual, whereas the last bits are obtained by considering a second-order Born approximation [20]:

$$E_{tot}^{v(K_0)}(x_n, y_n) = E_{inc}^v(x_n, y_n) + \sum_{p=1}^{N} \tau_{(c)}^{(opt)}(x_p, y_p) E_{inc}^v(x_p, y_p) \int_{D_p} G_{2D}(k_0 \rho_{np}) \, dx' dy' +$$

$$\sum_{p=1}^{N} \tau_{(c)}^{(opt)}(x_p, y_p) \left\{ \sum_{q=1}^{N} \tau_{(c)}^{(opt)}(x_q, y_q) E_{inc}^v(x_q, y_q) \int_{D_q} G_{2D}(k_0 \rho_{pq}) \, dx' dy' \right\} \int_{D_p} G_{2D}(k_0 \rho_{np}) \, dx' dy'$$

$$(8)$$

- the others $\left(\frac{N_p}{2} - 1 \right)$ chromosomes are randomly generated by considering multiple mutations in the Born-type chromosome.

4   Numerical Results

In the following, some numerical results are shown in order to assess the effectiveness but also current limitations of the proposed approach. Let us consider a square homogeneous cylinder l_D-sided with an area equal to A_D. M equally spaced measurement points are

located on a circle r in radius $(r > \frac{l_D}{\sqrt{2}})$. The values of the scattered electric field at the measurement points are synthetically obtained by the moment method. V incident plane waves are assumed: $E_{inc}^v(x,y) = e^{-jk_0(x\cos\vartheta_v + y\sin\vartheta_v)}$, where the angles $\vartheta_v = (v-1)\frac{2\pi}{V}$, $v = 1, ..., V$ define the propagation directions. As far as the parameters for the GA are concerned, the following values are chosen: $N_P = 80$, $P_c = 0.7$, $P_m = 0.4$, $P_{bm} = 0.01$, $K_{max} = 1000$.

4.1 Definitions

The signal-to-noise (SNR) ratio is defined as

$$SNR = 10log_{10}\frac{\sum_{v=1}^{V}\sum_{m=1}^{M}|E_{scatt}^v(x_m, y_m)|^2}{2MV\sigma_{noise}^2} \qquad (9)$$

where σ_{noise}^2 is the variance of the additive Gaussian noise with zero mean value.

The errors in the crack identification are quantified by the following figures.

1)   Error in the location of the center of the crack, δ_c:

$$\delta_c = \frac{\sqrt{(x_0 - \widehat{x}_0)^2 + (y_0 - \widehat{y}_0)^2}}{d_{max}} \times 100 \qquad (10)$$

being $(\widehat{x}_0, \widehat{y}_0)$ the estimated coordinates of the crack, and $d_{max} = \sqrt{2}l_D$ the maximum error in defining the crack center when it belongs to the host scatterer.

2)   The same error as in 1) but normalized to the wavelength:

$$\delta_0 = \frac{\sqrt{(x_0 - \widehat{x}_0)^2 + (y_0 - \widehat{y}_0)^2}}{\lambda_0} \times 100 \qquad (11)$$

3)   Error in the estimation of the crack area:

$$\delta_A = \frac{A_c - \widehat{A}_c}{A_c} \times 100 \qquad (12)$$

where $\widehat{A}_c$ and A_c are the estimated and actual crack areas, respectively.

11

4)   Errors in predicting the electric field are quantified by:

$$\Delta_{Etot}^{\nu}(x_n, y_n) = \frac{\left| \left| \widehat{E}_{tot}^{v}\left(x_n, y_n\right)\right| - \left|E_{tot}^{v}\left(x_n, y_n\right)\right|\right|}{\left|E_{tot}^{v}\left(x_n, y_n\right)\right|} \times 100 \qquad (13)$$

where $\widehat{E}_{tot}^{v}$ is the estimated electric field.

4.2 Crack Detection

In the first example, the aim is to explore the possibility of detecting the crack presence from the knowledge of the measured scattered electric field in a noisy environment characterized by different values of the signal-to-noise ratio. Let us consider a square object 0.214λ-sided, being λ the free-space wavelength corresponding to the working frequency f. The object is characterized by a dielectric permittivity $\varepsilon\left(x, y\right) = 2.0\varepsilon_0$. The scattered electric field is collected in $M = 81$ measurement points placed in a circle $r = \frac{32}{15}\lambda$ in radius and $V = 4$ views are considered. The coordinates of the center of the square crack are $x_0 = y_0 = \frac{\lambda}{30}$ and its area assumes different values. Figure $3(a)$ shows a color-level representation of the detection function for different values of the crack area and for various signal-to-noise ratios in the range $5 - 50dB$. We can observe that when the SNR is greater than $10dB$, as the crack area increases the detection function proportionally increases. On the contrary, when the noise amplitude increases, the value of $\Phi_{detection}$ tends to become more and more small and almost constant whatever the crack dimensions. Consequently, the possibility of detecting the presence of the crack is considerably reduced. As an example assuming a threshold value $\eta = 30$, the "$detection$ region" (defined as the range of values of SNR and A_c for which $\Phi_{detection} \geq \eta$) is limited to $SNR \geq 10.5$ for cracks of area greater than 10% of the area of the object cross section.

The effectiveness of the detection process is increased when an higher frequency is used as can be inferred from Figure $3(b)$ where a frequency $f_0 = 3f$ is considered. In this case, the values of the detection function are higher, even for SNR values less than $10dB$.

For $\eta = 30$, the detection area is limited by $SNR = 6dB$ and for cracks of area greater than 3% of the whole cross section.

4.3   Crack Identification.

In the first example, let us consider an object cross section $\frac{4}{5}\lambda_0$-sided, and a crack centered at point $x_0 = y_0 = \frac{\lambda_0}{10}$. The crack is square and its area is changed in the range between 0.1% to 10% of A_D. The measurement domain is a circle $r = \frac{16}{25}\lambda_0$ in radius. SNR varies between $5dB$ and $50dB$. Figure 4 shows the error figures in the crack identification and field prediction. Since the GA-based procedure is non-deterministic, each data point in the following figures is based on the average of the results obtained with twenty independent runs of the algorithm. Therefore slight variations may be observed among curves representing runs with similar parameters. From Figure 4, it can be observed that the errors in the center location are less than 3% of d_{max} for all the cracks when $SNR \geq 20dB$ and for crack with area greater than 4% of A_D when $SNR \geq 6dB$. For the region defined by $8dB \leq SNR \leq 20dB$ and $2 \times 10^{-3} \leq \frac{A_c}{A_D} \leq 4 \times 10^{-2}$, a greater error results ($\delta_c \cong 10$). The crack location results very difficult otherwise. Figure 4(b) gives an idea of the evaluation of the crack area performed by the algorithm. It can be observed that the distribution of the amplitude of δ_A is similar to that of δ_c, but generally the error values are greater.

The third example is aimed at assessing the effectiveness of the algorithm for different crack positions inside the host medium. The position of a crack with an area equal to $0.04A_D$ is changed along the diagonal of the square investigation domain. All the plots reported in Figure 5 show that the reconstruction is independent of the position of the crack. The amplitude of the errors are determined from the signal-to-noise value. In particular, $\delta_c \leq 10$, $|\delta_A| \leq 20$, and $\delta_{Etot} \leq 2$ for $SNR \geq 14dB$.

The effectiveness of the algorithm in locating the crack is then evaluated when the

dimensions of the object cross section are changed. A square crack $0.05\lambda_0$-sided and located in $x_0 = y_0 = \frac{l_D}{4}$ is considered. Figure 6 gives the plot of δ_0 for different dimensions of l_D and for various values of SNR. The center of the crack is determined with great accuracy for $0.1 \leq \frac{l_D}{\lambda_0} \leq 1.0$ ($\delta_0 \leq 10$). For greater dimensions of the investigation domain, the error increases about linearly ($\delta_0 = 114\frac{l_D}{\lambda_0} - 100$).

In order to give some indications about the iterative process, Figure 7 shows the behavior of the fitness function versus the iteration number for the same geometry considered in the previous example and for a noiseless case. The decreasing of the fitness function in correspondence with the best individual ($\Phi_{identification}\{\psi^{opt}\}$) is about three order of magnitude in the first 400 iterations. Then the rate of convergence considerably reduces and the *refresh* procedure operates according to the rule stated in Section 3. Generally, large variations in the average of the fitness values of the individuals of the population ($< \Phi_{identification}\{\psi_k\} >$) are due to the generation of new individuals which are very different from the other individuals of the previous population. The mutation but especially the refresh procedure are responsible of this fact. For completeness also the plots of the two terms of the identification function are shown.

An idea of the data fitting obtained with the presented approach is given in Figure 8, where the amplitude of the estimated scattered electric field ($\nu = 1$) in the observation domain is presented for different noisy cases. In all cases the agreement between measured and reconstructed amplitude profiles is quite good starting from the iteration $k = 100$.

Figure 9 gives the plot of the error in estimating the crack area during the iterative process, respectively. It should be pointed out that, starting from $k = 100$, the center of the crack is located quite correctly and $\delta_c \leq 10$ whatever the noisy case considered. On the contrary, the estimation of the area of the crack results more difficult and the final reconstruction is performed with an error amplitude which ranges from $|\delta_A| = 0$ to $|\delta_A| = 25$ ($SNR = 20dB$).

Finally, Figure 10 gives an idea of the prediction of the electric field distribution

14

inside the investigation domain during the iterative process. Figures $10(a)$ and $10(b)$ show the amplitude of field distribution for the crack free configuration and with the crack, respectively. In the following, the error $\Delta_{Etot}^{\nu}(x_n, y_n)$, $\nu = 1$ in reproducing the actual distribution is reported at the iterations $k = 0$ (Fig. $10(c)$), $k = 100$ (Fig. $10(d)$), $k = 300$ (Fig. $10(e)$), and $k = 800$ (Fig. $10(f)$). As can be seen, initially the prediction is very poor and related errors are large. Starting from iteration $k = 100$ the estimated values of the electric field tend to become more and more similar to the actual ones. The not uniform distribution that the error keeps at the first iterations (Figs. $10(c)$-(d)), tends to disappear as k increases, as shown in Figure $10(e)$ and the solution agree very well with the reference one as clearly indicated in Figure $10(f)$.

5   Conclusions

A microwave imaging approach has been applied for 2D crack detection using synthetic data. An iterative procedure based on a genetic algorithm which allows for an use of the a-priori knowledge, has been presented. Particular attention has been devoted to choose an appropriate representation of the unknowns of the problem and suitable genetic operators have been defined. The validity of the approach has been verified by using noisy data and current limitations pointed out. In order to avoid these drawbacks and increase the range of the applicability of the proposed approach, further investigations will be devoted to define suitable penalty terms in order to favor a physically reasonable solution.

References

[1] R. Zoughi, "Recent advances in near-field microwave and millimeter wave nondestructive testing and evaluation techniques" in *Proc. AP2000*, Davos, Switzerland, 2000.

[2] M. Bramanti and E. Salerno, "Electromagnetic techniques for nondestructive testing of dielectric materials: Diffraction tomography," *Journal of Microwave Power*, vol. 27, no. 4, 1992.

[3] N. Qaddoumi, S.I. Ganchev, G. Carriveau and R. Zoughi, "Microwave imaging of thick composites with defects," *Materials Evaluation*, vol. 53, no. 8, pp. 926-929, Aug. 1995.

[4] K. Belkebir, C. Pichot, J. C. Bolomey, P. Berthaud, G. Cottard, X. Derobert, and G. Fauchoux, "Microwave tomography system for reinforced concrete structures," in *Proc. 24th EuMC*, vol. 2, pp. 1209-1214, 1994.

[5] A. Joisel, J. Mallorquì, A. Broquetas, J. M. Geffrin, N. Joachimowicz, M. Vallilossera, L. Jofre, and J. C. Bolomey "Microwave imaging techniques for biomedical applications," in *Proc. IMTC'99*, Venice, Italy, pp. 1591-1596, 1999.

[6] A. Ishimaru, *Electromagnetic Wave, Propagation, Radiation and Scattering.* Prentice-Hall, 1991.

[7] J. H. Richmond, "Scattering by a dielectric cylinder of arbitrary cross-section shape," *IEEE Trans. Antennas Propagat.*, vol. 13, pp. 334-341, 1965.

[8] D. E. Goldberg, *Genetic Algorithms in Search, Optimization, and Machine Learning*, Addison-Wesley, Reading, Mass., 1989.

[9] S. Caorsi, A. Massa, and M. Pastorino, "Genetic algorithms as applied to the computation of electromagnetic scattering by weakly nonlinear dielectric cylinders," *IEEE Transactions on Antennas and Propagation*, vol. 47, no. 9, pp. 1421-1428, 1999.

[10] J. H. Holland, *Adaptation in Natural and Artificial Systems. Ann Arbor*: Univ. Michigan Press, 1975.

[11] R. L. Haupt, "An introduction to genetic algorithms for electromagnetics," *IEEE Antennas Propagat. Magazine*, 37, 2, 7-15, 1995.

[12] D. S. Weile and E. Michielssen, "Genetic algorithm optimization applied to electromagnetics: a review," *IEEE Trans. Antennas Propagat*, vol. 45, pp. 343-353, March 1997.

[13] L. J. Eshelman and J. D. Schaffer, "Real-coded genetic algorithms and interval-schemata," in *Foundations of Genetic Algorithms 2*. S. Forrest, Ed. San Mateo, CA: Morgan Kaufmann, 1993, pp. 187-202.

[14] C. Z. Janikow and Z. Michalewicz, "An experimental comparison of binary and floating point representations in genetic algorithms," in *Foundations of Genetic Algorithms 2*. S. Forrest, Ed. San Mateo, CA: Morgan Kaufmann, 1993, pp. 31-36.

[15] N. J. Radcliffe, "Equivalence class analysis of genetic algorithms," *Complex Systems*, vol. 5, no. 2, pp. 183-206, 1991.

[16] A. H. Wright, "Genetic algorithms for real parameter optimization," in *Foundations of Genetic Algorithms 2*. S. Forrest, Ed. San Mateo, CA: Morgan Kaufmann, 1993, pp. 205-218.

[17] D. B. Fogel, "An introduction to simulated evolutionary optimization", *IEEE Trans. Neural Networks*, NN-5, pp. 3-14, 1994.

[18] D. E. Goldberg and K. Deb, "A comparative analysis of selection schemes used in genetic algorithms," *Foundations of Genetic Algorithms*, Morgan Kaufmann, 1991, pp. 69-93.

[19] J. M. Johnson and Y. Rahmat-Samii, "Genetic algorithms in engineering electromagnetics," *IEEE Trans. Antennas Propagat. Magaz.*, vol. 39, no.4, pp. 7-25, 1997.

[20] S. Caorsi, A. Massa, and M. Pastorino, "Iterative numerical computation of the electromagnetic fields inside weakly nonlinear infinite dielectric cylinders of arbitrary cross sections using the distorted-wave Born approximation", *IEEE Transactions on Microwave Theory and Techniques*, vol. 44, no. 3, pp. 400-412, 1996.

FIGURE CAPTIONS

- Figure 1.

  Problem Geometry.

- Figure 2.

  Example of a *chromosome* used in the genetic algorithm procedure.

- Figure 3.

  Color-scale representation of the detection function. (a) Operating frequency f. (b) Operating frequency $f_0 = 3f$.

- Figure 4.

  Errors in the reconstruction for different areas of the crack and for different values of the signal-to-noise ratio: (a) δ_c, and (b) $|\delta_A|$.

- Figure 5.

  Errors in the reconstruction for different positions of the crack and for different values of the signal-to-noise ratio: (a) δ_c, and (b) $|\delta_A|$.

- Figure 6.

  Plot of the localization error, δ_0, versus the side dimension of the host object.

- Figure 7.

  Behavior of the fitness function versus the number of iterations.

- Figure 8.

  Amplitude of the scattered electric field in the observation domain. Actual, crack-free and reconstructed field distributions (k iteration number). (a) $SNR = 40db$ and (b) $SNR = 20db$.

- Figure 9.

  Behavior of the error parameters in (a) the crack localization and in (b) the crack sizing versus the number of iterations and for different signal-to-noise ratio.

- Figure 10.

  Prediction of the electric field inside the investigation domain. Images of the electric field amplitude for (a) the crack- free case and (b) with the crack. Images of the error $\Delta_{Etot}^{\nu}(x_n, y_n)$, $\nu = 1$, at the iteration: (c) $k = 0$, (d) $k = 100$, (e) $k = 300$, and (f) $k = 800$.
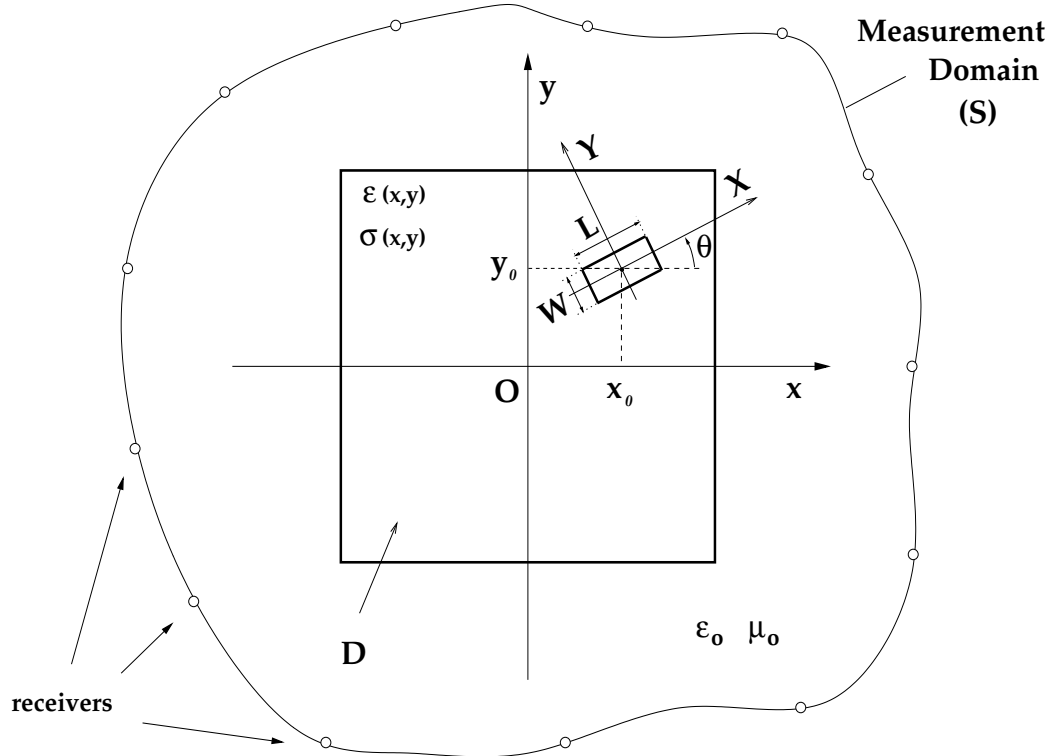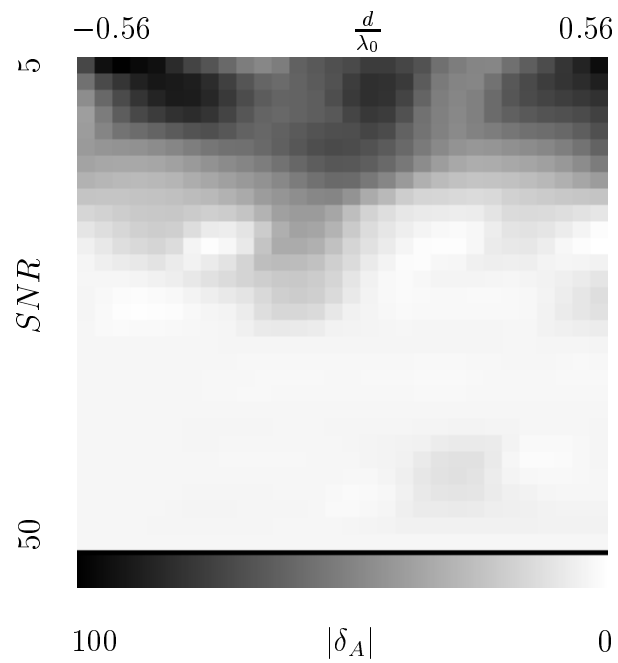
Fig. 1 - S. Caorsi et al. "A Crack Identification Microwave Procedure ..."

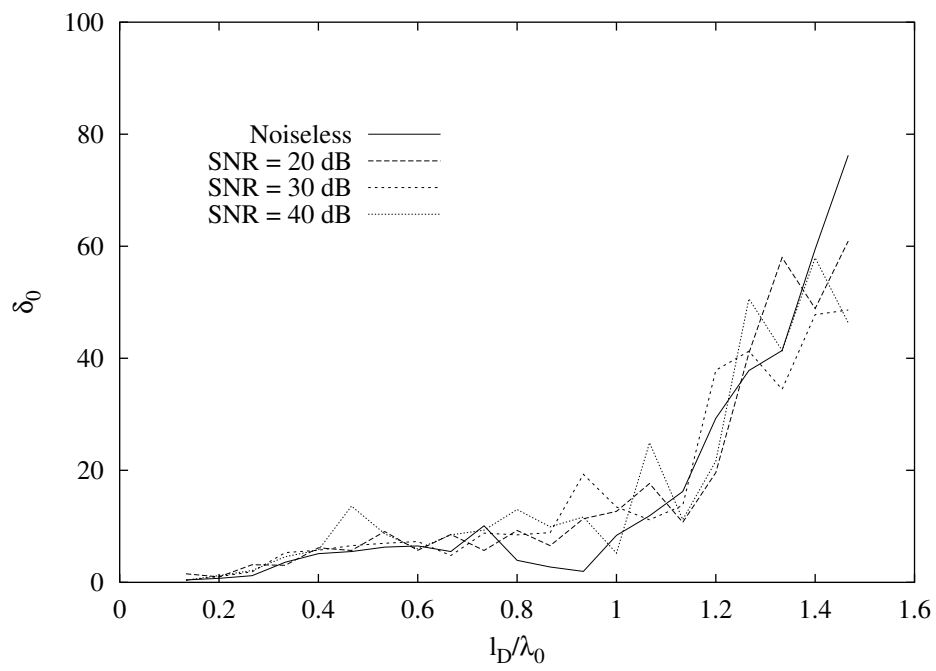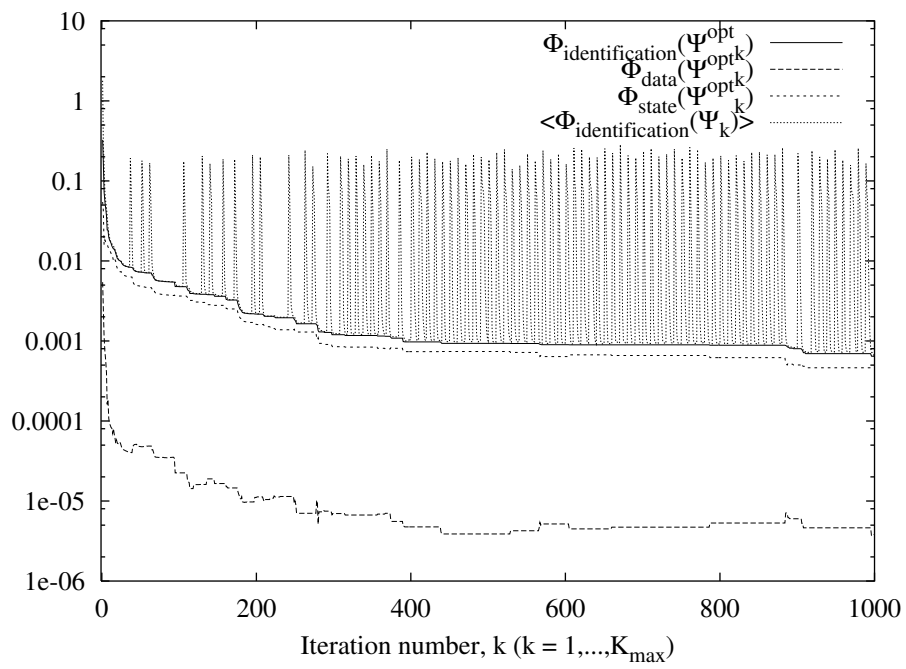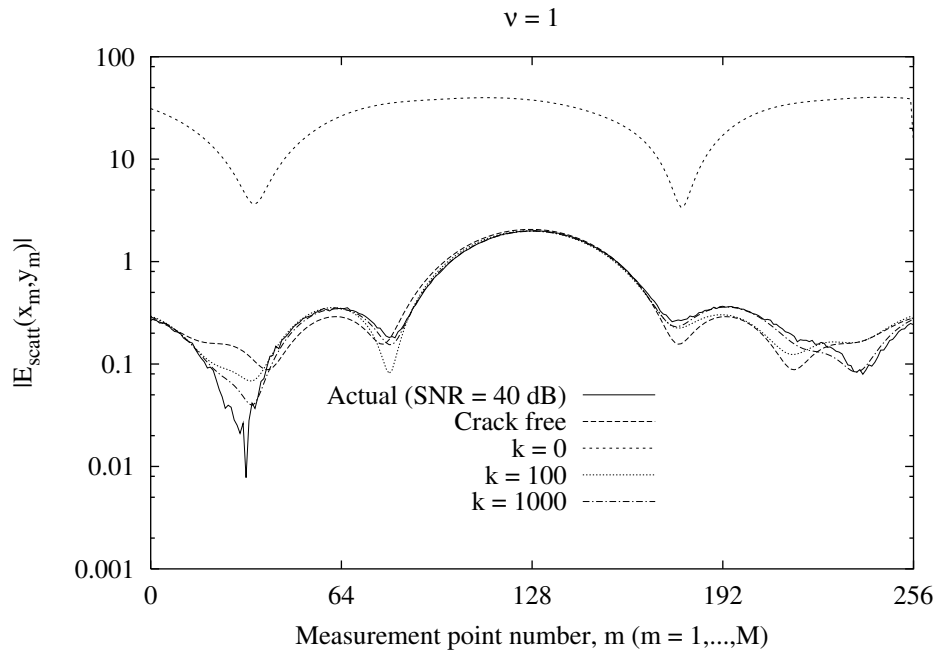Fig. 2 - S. Caorsi et al. "A Crack Identification Microwave Procedure ..."

$\frac{A_c}{A_D}$ (%)

SNR

$\Phi_{detection}$

(a)

$\frac{A_c}{A_D}$ (%)

SNR

$\Phi_{detection}$
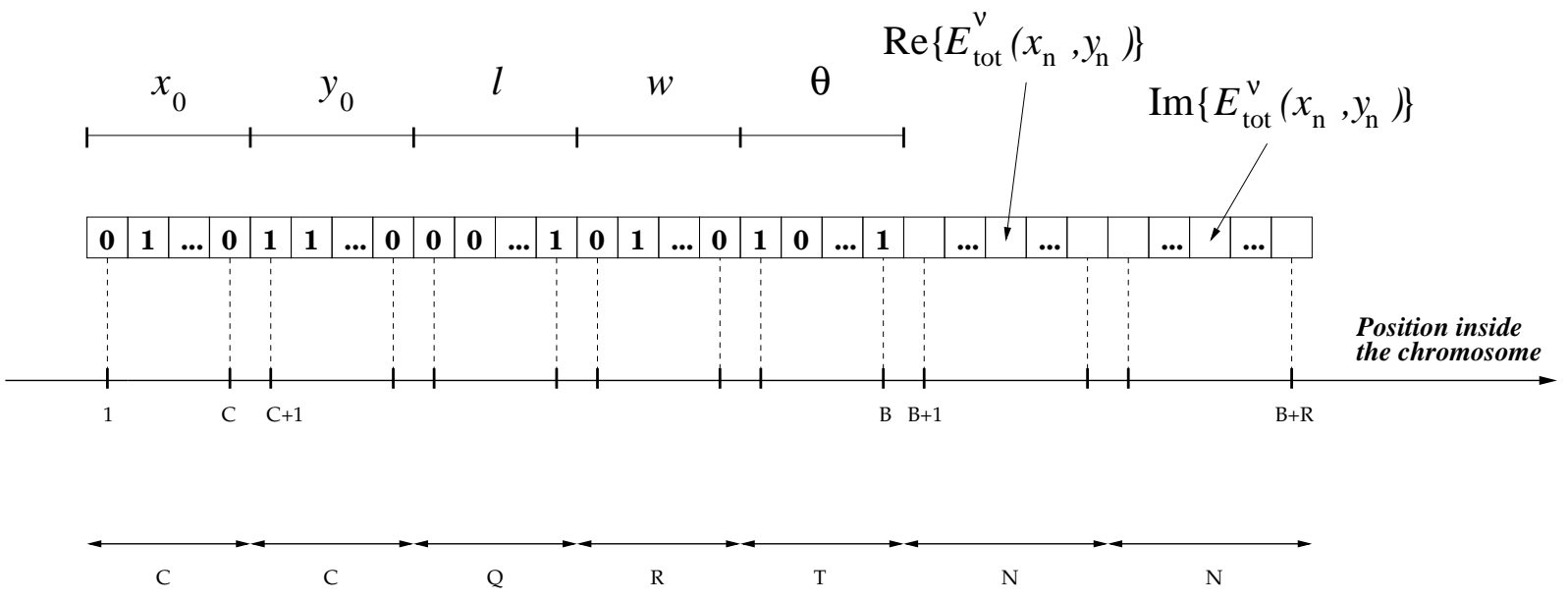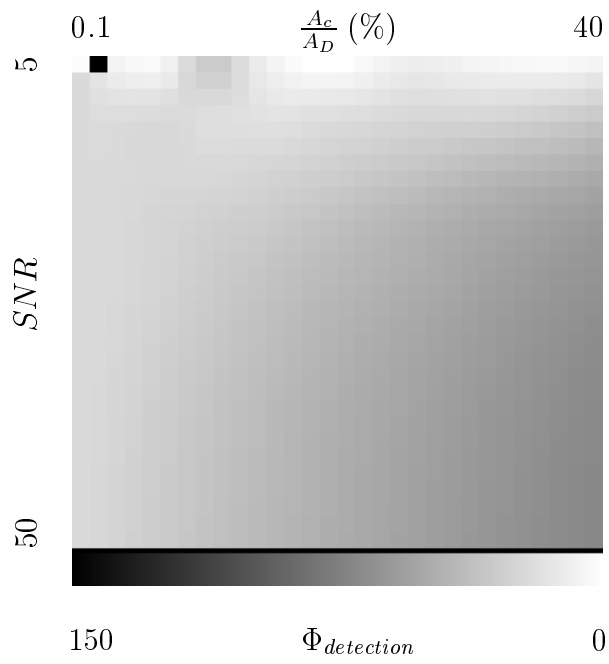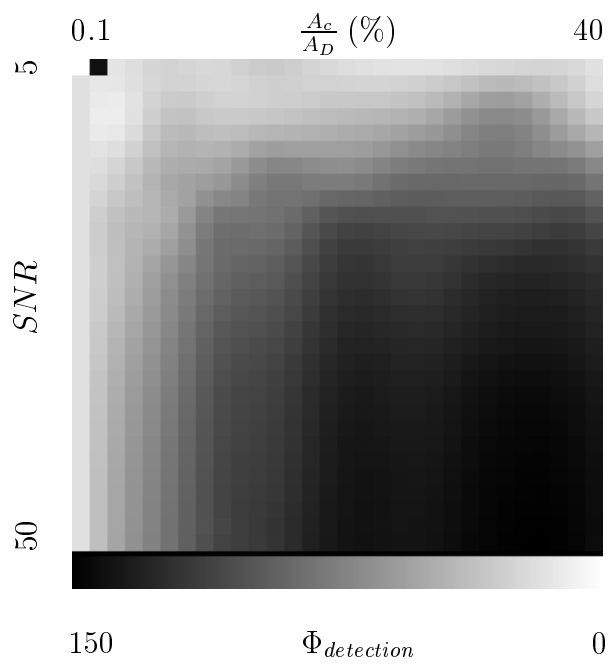
(b)

Fig. 3 - S. Caorsi et al. "A Crack Identification Microwave Procedure ..."

(a)

(b)

Fig. 4 - S. Caorsi et al. "A Crack Identification Microwave Procedure ..."

$$-0.56 \qquad \frac{d}{\lambda_0} \qquad 0.56$$

$$50 \qquad \delta_c \qquad 0$$

(a)

$$-0.56 \qquad \frac{d}{\lambda_0} \qquad 0.56$$

$$100 \qquad |\delta_A| \qquad 0$$
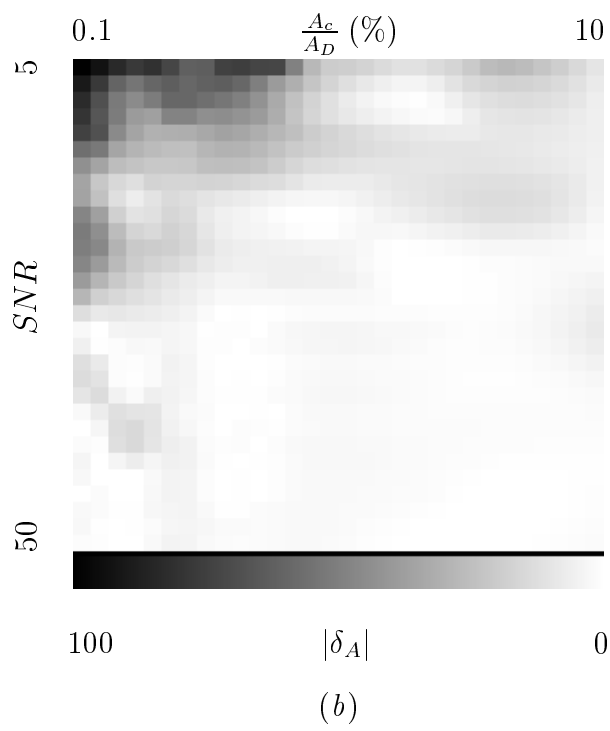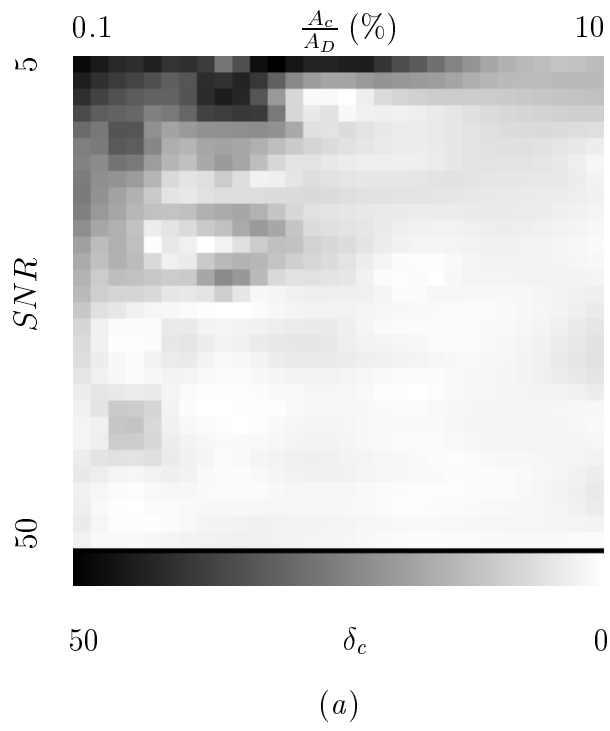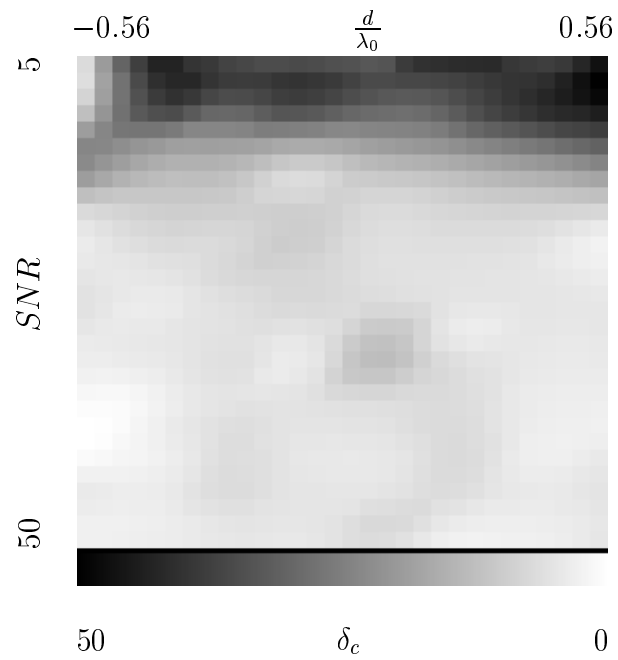
(b)

Fig. 5 - S. Caorsi et al. "A Crack Identification Microwave Procedure ..."

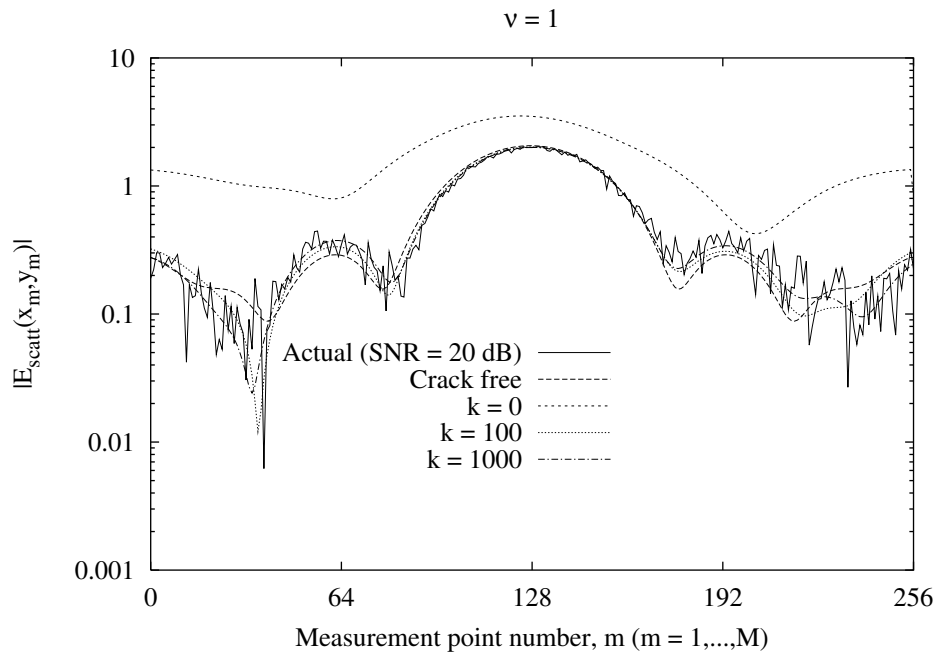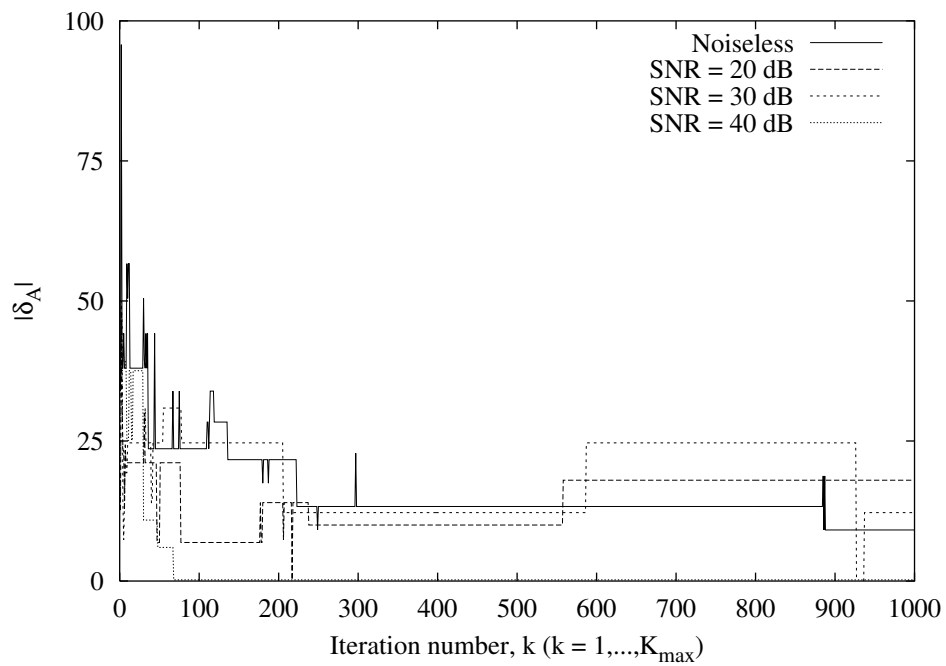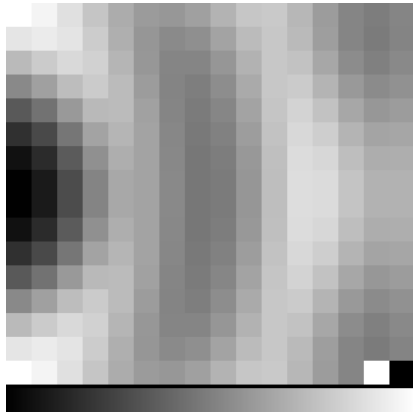**Fig. 6 - S. Caorsi et al.** "A Crack Identification Microwave Procedure ..."

26

The plot legend reads:

$\Phi_{identification}(\Psi^{opt})$
$\Phi_{data}(\Psi^{opt k})$
$\Phi_{state}(\Psi^{opt}_k)$
$<\Phi_{identification}(\Psi_k)>$

The y-axis is labeled with values: 10, 1, 0.1, 0.01, 0.001, 0.0001, 1e-05, 1e-06.

The x-axis is labeled: Iteration number, k (k = 1,...,K_{max}) with values 0, 200, 400, 600, 800, 1000.

Fig. 7 - S. Caorsi et al. "A Crack Identification Microwave Procedure ..."

$\nu = 1$

$|E_{scatt}(x_m,y_m)|$

Measurement point number, m (m = 1,...,M)

Actual (SNR = 40 dB)
Crack free
k = 0
k = 100
k = 1000

(a)

$\nu = 1$

$|E_{scatt}(x_m,y_m)|$

Measurement point number, m (m = 1,...,M)

Actual (SNR = 20 dB)
Crack free
k = 0
k = 100
k = 1000

(b)

Fig. 8 - S. Caorsi et al. "A Crack Identification Microwave Procedure ..."

(a)

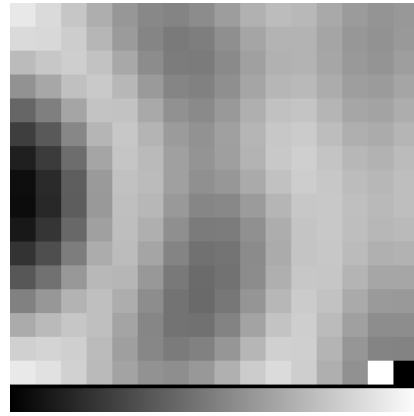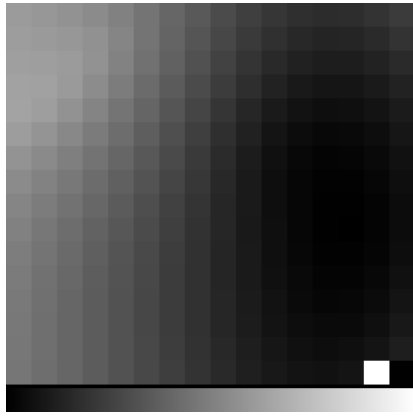**Fig. 9 - S. Caorsi et al.** "A Crack Identification Microwave Procedure ..."
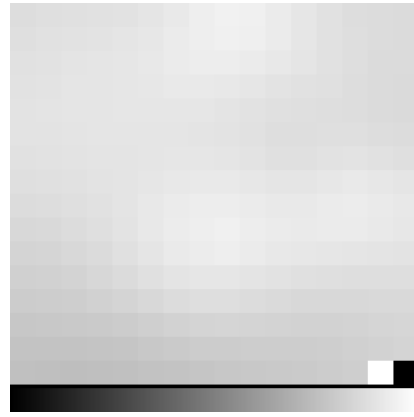
2.00 $|E^1_{tot}(x_n, y_n)|$ 0.40 2.00 $|E^1_{tot}(x_n, y_n)|$ 0.40

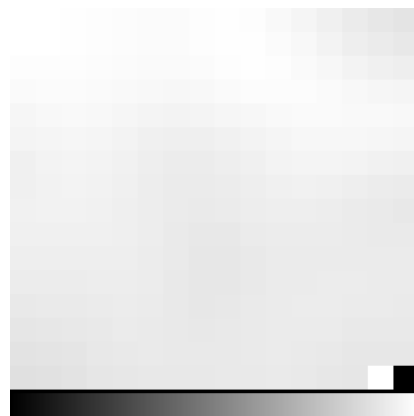(a) (b)

28 $\Delta^1_{Etot}(x_n, y_n)$ 1.4 28 $\Delta^1_{Etot}(x_n, y_n)$ 1.4

(c) (d)

28 $\Delta^1_{Etot}(x_n, y_n)$ 1.4 28 $\Delta^1_{Etot}(x_n, y_n)$ 1.4

(e) (f)

30

Fig. 10 - S. Caorsi et al. "A Crack Identification Microwave Procedure ..."